Chemical Engineering Journal 152 (2009) 543–555

Contents lists available at ScienceDirect

Chemical Engineering Journal

journal homepage: www.elsevier.com/locate/cej

Optimization of a novel combination of fixed and fluidized-bed hydrogen-permselective membrane reactors for Fischer–Tropsch synthesis in GTL technology

M.R. Rahimpour*, H. Elekaei

Chemical Engineering Department, School of Chemical and Petroleum Engineering, Shiraz University, Shiraz 71345, Iran

ARTICLE INFO

Article history:
Received 19 December 2008
Received in revised form 11 May 2009
Accepted 12 May 2009

Keywords:
Fischer–Tropsch synthesis
Fluidized-bed
Membrane reactor
FTS reactor combination
Optimization
Genetic algorithm

ABSTRACT

In this work, a novel combination of fixed and fluidized-bed hydrogen-permselective membrane reactors for Fischer–Tropsch synthesis (FTS) has been optimized using Genetic Algorithm (GA). This novel reactor configuration incorporates a fixed-bed FTS reactor with a membrane assisted fluidized-bed FTS reactor. In the proposed configuration, hydrogen is withdrawn from the fresh feed synthesis gas and is injected to the end segment of reactor in order to control dozing of hydrogen along the reactor and prevention of hydrogen waste. A theoretical investigation was performed in order to optimize the reactor performance, maximizing C_5^+ production and at the same time, minimizing the CO_2 yield as an undesired product. The optimization was carried out and the results show there is a favorable profile of FTS products along the optimized combined system relative to the conventional fixed-bed single stage FTS reactor. Optimal ratio of reactors length, H_2/CO ratio, catalyst size, shell and tube pressures of second reactor, hydrodynamic parameters, gas phase velocity and temperature profile along the reactor were obtained and 45.9% additional C_5^+ yield was resulted in optimized system relative to conventional fixed-bed single stage FTS reactor.

1. Introduction

The Fischer–Tropsch synthesis (FTS) refers to the conversion of synthesis gas ($CO + H_2$) into hydrocarbons such as C_5^+ and diesel [1]. FTS has become a subject of renewed interest in recent years due to an escalation in the price of oil and the discovery of several gas reserves. Parts of the world gas reserves are located in remote areas and several of them are in offshore regions so that transport of natural in these cases can become expensive and uneconomical. The FTS can be used to convert natural gas into liquid hydrocarbons, making transport much easier and economical. Furthermore, a great part of the world energy source is based on liquid hydrocarbons such as C_5^+, kerosene, and diesel, so that conversion of natural gas into liquid transportation fuels is interesting for many countries and oil companies [2]. Due to the high demand on C_5^+ in the world and its higher price relative to that of diesel, production of C_5^+ from the FT process, becomes more favorable. The octane number of C_5^+ from FTS is lower than that of the C_5^+ obtained from crude oil processing, since the C_5^+ from FTS mainly consists of n-paraffin. To promote the yield and quality of the C_5^+ from Fischer–Tropsch synthesis, bifunctional catalysts have received extensive attention in the recent years [3].

The various types of reactors (including fixed-bed, fluidized-bed, ebulliating-bed, and slurry phase) have been considered in the history of FTS process development, characterizing with the most suitable particle size of the catalyst used [4]. FTS is either low temperature process (LTFT) or high temperature process (HTFT) depending on the product required. High temperature process operates at 300–350 °C on Fe-based catalysts and is mainly used for the production of C_5^+ and linear olefins while low temperature process operates at 200–240 °C and is applied for the production of waxy material [5]. The LTFT synthesis takes places in a three-phase system. The gas phase contains the reactants and water vapor and gaseous hydrocarbon products. The higher hydrocarbons compose the liquid phase, and the catalyst is the solid phase. During HTFT, all of the products are often vaporized under reaction conditions and so there are only two phases presents [5].

Conventional fixed-bed reactors are seriously limited by poor heat transfer and low catalyst particle effectiveness factors because of severe diffusional limitations with the catalyst particle sizes used. Smaller particle sizes are infeasible in fixed-bed systems because of pressure drop considerations [6]. In order to avoid serious pressure drop, the effective diameter of catalyst particles in fixed-bed reactor is usually over 2.5 mm, which brings a certain inner mass transfer resistance.

* Corresponding author. Tel.: +98 711 2303071; fax: +98 711 6287294.
E-mail address: rahimpor@shirazu.ac.ir (M.R. Rahimpour).

1385-8947/$ – see front matter © 2009 Elsevier B.V. All rights reserved.
doi:10.1016/j.cej.2009.05.016

A single stage fixed-bed FTS (FixS) was developed in the Research Institute of Petroleum Industry (RIPI) to produce high octane number and low sulfur C_5^+ by a modified bifunctional Fe-HZSM5 catalyst. Such a process removes the need for a cumbersome upgrading unit for GTL plants [7]. Ahmadi Marvast et al. simulated the RIPI single stage fixed-bed FTS reactor [8]. The simulation results showed a negligible change in temperature and concentration profiles over 7 m reactor length. Likewise, it has been observed that the reacting gas is H_2-poor in the second half of the reactor and hydrogen adding into the system is necessary. "H_2-poor" means that the H_2/CO ratio is lower than the optimum ratio what is required for C_5^+ production.

In this study, aforesaid reactor is divided in two reactors. First reactor is similar to that of RIPI with exception of having 7.2 m length. A bubbling fluidized-bed membrane reactor concept is proposed for second reactor [9,10] to incorporate hydrogen-permselective membrane, controlled dosing capabilities of hydrogen with membrane, and excellent heat and mass transfer capabilities of fluidized-bed. In this way hydrogen is re-distributed along the reactor so that the amount of hydrogen fed to the inlet of reactor is reduced and the amount of hydrogen at the last segment of reactor is increased. Therefore the proposed system which is a fluidized-bed membrane dual-type (FMD) reactor is a shell and tube heat exchanger that a fixed-bed water-cooled reactor is combined in series with a fluidized-bed membrane reactor. Fresh synthesis gas is preheated inside the tubes of the second reactor and then is fed into the tubes of the water-cooled reactor. Here, the chemical reactions are initiated by the catalyst and synthesis gas is partly converted to FTS products. The reacting gas leaving the water-cooled reactor is directed into the shell side of the second reactor which is a fluidized-bed membrane reactor. This reacting gas is flowing through the fluidized-bed in counter-current mode with fresh synthesis gas flowing through the tubes and the reactions are completed in the second reactor [11]. Due to highly exothermic chemical reactions, the fluidized-bed concept [12] is considered for the second reactor. The wall of the tubes in the second reactor is coated with the permselective Pd–Ag membrane which transmits hydrogen to the reaction side of last segment of reaction side as a result of hydrogen partial pressure driving force. Therefore ratio of hydrogen to carbon monoxide is controlled along the reactors.

This reactor configuration solves some observed drawbacks of industrial fixed-bed FTS reactors such as pressure drop, heat transfer problem, internal mass transfer limitations and radial gradient of concentration and temperature. The phenomenon of hydrogen-permselective Pd–Ag membrane is used to obtain a major increase in production rate by stoichiometric control of reacting gases. By insertion of membranes in a fluidized-bed both optimal concentration profiles via controlled dosing of hydrogen and a uniform temperature along the reactor can be created, so that large improvements in conversion and selectivity could be achieved. In this respect, the suggested reactor system prevents higher damage to the membrane wall as a result of very good heat transfer and temperature equalization characteristics of fluidization. Considerable attention has been paid to the fluidized-bed membrane reactors as multi-functional reactors because of their main advantages such as enhancement of conversion, best reactants molar ratio on the catalytic surface, simultaneous reaction and separation of hydrogen, elimination of diffusion limitations, superior heat transfer capability and a more compact design [13,14].

Fluidized-bed reactors operate at relatively high temperature and moderate pressure, producing a relatively light product economically (mostly C_5^+ or lighter hydrocarbons). Fluidized-bed membrane reactors can be considered in terms of bubbling regime, turbulent regime, or fast fluidization regime. The choice is likely to be dictated by competing factors such as compactness, temperature uniformity, high bed-to-tube heat transfer, and limitation of the forces on and erosion of the membrane surfaces. The latter factor is likely to be favored by high-velocity regimes (turbulent or fast fluidization), while the bubbling-bed regime may be best in terms of the other criteria. So far, all fluidized-bed membrane reactors experiences have been in bubbling beds [15]. So, we discuss our concept in terms of the bubbling-bed regime in this research.

In literature, simulation studies with fluidized-bed Fischer–Tropsch reactor are quite limited. Liu et al. experimentally developed and demonstrated a novel dry fluidized-bed reactor system (called "heat tray") for FT synthesis from a low H_2/CO gas [16]. The results indicated very high heat transfer coefficients between a shallow bed and its immersed horizontal heat-transfer tube. Then, Sasol R&D investigated a fluidized-bed system for FTS pilot plant due to increase the production capacity and overcome the limitations of Synthol CFB reactor and designed a full scale commercial unit which came on stream in mid-1989. Higher conversions and yields were achieved compared to the CFB Synthol units. Sasol demonstrated that the cost of the new reactor is half of that of an equal capacity CFB unit [12,17].

In this work, we aim to maximize the production of high octane C_5^+ on bifunctional Fe-HZSM5 catalyst through HTFT process in the fixed-bed cascading with bubbling fluidized-bed membrane reactor. So, initially, this proposed concept is mathematically modeled and pursuant to simulation, an optimization approach is applied to determine the optimum fluidization conditions and catalyst size, the best ratios of H_2/CO and reactors lengths, the most appropriate pressures of second reactor and finally the optimal cooling water and feed gas temperature. Optimization tasks are investigated by novel optimization tools, genetic algorithms. Genetic algorithms are imitation of natural evolution and are believed as powerful optimization techniques among stochastic methods [18]. Consequently, maximum production rate of C_5^+ in proportion to utmost conversion of CO_2 to FTS products is obtained. A comparative study is carried out to compare the performance of optimized fluidized-bed dual-type (OFD) and optimized fluidized-bed membrane dual-type (OFMD) reactor with conversional fixed-bed single stage (FixS), respectively. Also, fluidized-bed dual-type reactor (FD) resembles to FMD system with no membrane. Therefore, the FD model is same as FMD model unless H_2 permeation rate equals to zero.

2. Genetic algorithm

Genetic algorithm (GA) is a class of probabilistic optimization algorithms, inspired by the biological evolution process. GA maintains a population of candidate solutions for the problem at hand and makes it evolve by iteratively applying a set of stochastic operators. The first step in optimization is defining the objective function and its decision variables constrained depending on the type of problem in hand. These constraints will form penalty functions which should be considered in the mentioned method.

Basic components of GA are gene, chromosome and population. Gene is any decision variable. Chromosome is any complete set of genes. Therefore, objective function is a function of chromosomes. Population is defined as a set of chromosomes [19].

3. Process description

As will be described in later sections, the Fischer–Tropsch synthesis has been investigated in a fixed-bed single stage and fixed-bed cascading with fluidized-bed membrane reactor which they are packed with bifunctional Fe-HZSM5 catalyst (metal part: 100 Fe/5.4 Cu/7 K_2O/21 SiO_2, acidic part: SiO_2/Al_2O_3 = 28). The optimum conditions of this catalyst have been determined to be 300 °C, 17 bars and the inlet H_2/CO ratio of 0.96 to get maximum C_5^+ production [7].

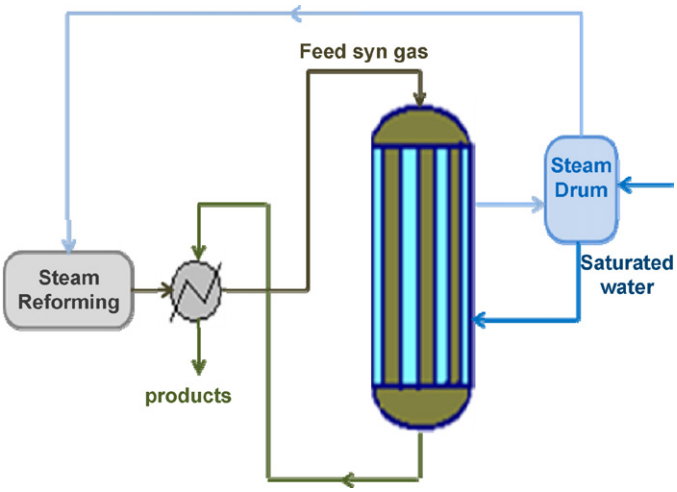

Fig. 1. Schematic diagram of a fixed-bed single stage Fischer–Tropsch synthesis reactor (FixS).

Table 1
FTs pilot plant characteristics.

Parameter	Value
Tube dimension [mm]	Ø38.1 × 3 × 6000
Molar ratio of H_2/CO in feed	0.96
Feed temperature [K]	569
Reactor pressure [kPa]	1700
Cooling temperature [K]	566.2
Catalyst sizes [mm]	Ø2.51 × 5.2
Catalyst density [kg m^{-3}]	1290
Bulk density [kg m^{-3}]	730
Number of tubes	1
Tube length [m]	12
GHSV [h^{-1}]	235
Bed voidage	0.488
Feed molar flow rate [gmol/s]	0.0335

3.1. Conventional fixed-bed FTS reactor (FixS)

In industrial fixed-bed Fischer–Tropsch reactors, multi-tubular reactors cooled by pressurized boiling water are often used. Fig. 1 shows a schematic of the fixed-bed multi-tubular FTS reactor. Table 1 presents the characteristics of the fixed-bed single stage industrial reactor [7,8].

3.2. Fixed-bed cascading with fluidized-bed membrane reactor (FMD)

Fig. 2 shows the schematic diagram of a fixed-bed cascading with fluidized-bed membrane reactor configuration for Fischer–Tropsch synthesis. Fundamentally, this system is based on the two-stage reactor consisting of a water-cooled and a synthesis gas-cooled reactor. The vertical tubes of fixed-bed reactor and shell side of fluidized-bed reactor are packed by catalysts. As shown in Fig. 2, firstly, the feed synthesis gas is flowing through the tubes of fluidized-bed reactor from upside. The walls of these tubes consist of hydrogen-permselective membranes. Thus, the mass and heat transfer processes simultaneously occur between both sides and hydrogen permeation arisen from hydrogen partial pressure gradient can improve the products yields. This simulation study is based on a Pd–Ag layer thickness of 1.2 μm. Then, the preheated synthesis gas is fed to the tubes of the water-cooled reactor and the chemical reaction is initiated by the catalyst. As known, FT synthesis reactions are highly exothermic and so, the cooling water in the shell side of fixed-bed reactor discharges the heat of reactions. In this stage, the partial conversion of synthesis gas to FT synthesis products is accomplished. The reacting gas containing hydrocarbons leaves the fixed-bed reactor and enters into the bottom of the fluidized-bed. The reacting materials flowing up through the fluidized-bed is in contact with fresh synthesis gas which is flowing downward through the tubes. The chemical reactions are continued on the catalyst surfaces in fluidized-bed system and the generated heat is removed by synthesis gas in tubes. Therefore, the reacting gas temperature is continuously reduced through the reaction path in the fluidized-bed reactor [11,20]. Finally, the products are transferred to Hydro Cracking Unit.

The all specifications of the water-cooled reactor in fixed-bed cascading with fluidized-bed membrane configuration are same as fixed-bed single stage FTS reactor with exception of reactor length. The length of fixed-bed reactor of the combined reactors has been selected 7.2 m.

Our concept plans to combine the advantages of combination of fixed and fluidized-beds reactors with hydrogen-permselective membrane to achieve higher conversion of synthesis gas to relatively light hydrocarbons such as C_5^+. Catalyst characteristics and specifications of fixed-bed cascading with fluidized-bed membrane reactor have been listed in Table 2.

4. Mathematical model

A one-dimensional heterogeneous model comprising a set of heat and mass transfer equations and the kinetics of the main reactions are chosen in this work to simulate the combination of fixed and fluidized-bed membrane reactors.

4.1. Reaction network

The Fischer–Tropsch components include H_2, CO, CO_2, H_2O, CH_4, C_2H_6, C_3H_8, n-C_4H_{10}, i-C_4H_{10} and C_5^+. The following reactions are

Table 2
Catalyst and specifications of fixed-bed cascading with fluidized-bed membrane reactor.

	Water-cooled reactor (first reactor)	Gas-cooled reactor (second reactor)
Catalyst density [kg m^{-3}] [7]	1290	1290
Catalyst equivalent diameter [m]	3.83 × 10^{-3} [6]	0.2 × 10^{-3} [25]
Molar ratio of H_2/CO in feed [7]	0.96	–
flow rate per tube [gmol s^{-1}]	0.0335 [7]	0.377
Feed temperature [K] [6]	565	–
Reactor pressure [kPa] [6]	1700	2200
Cooling temperature [K] [6]	566	–
Bulk density [kg m^{-3}] [6]	730	-
Tube length [m]	7.2	4.8
Tube size [mm]	Ø21.2 × 4.2	Ø21.2 × 4.2
Number of tubes	180	16
Bed voidage	0.488 [6]	0.56 (min fluidization)
Catalyst thermal conductivity [kJ m^{-1} s^{-1} K^{-1}] [6]	0.00625	0.00625

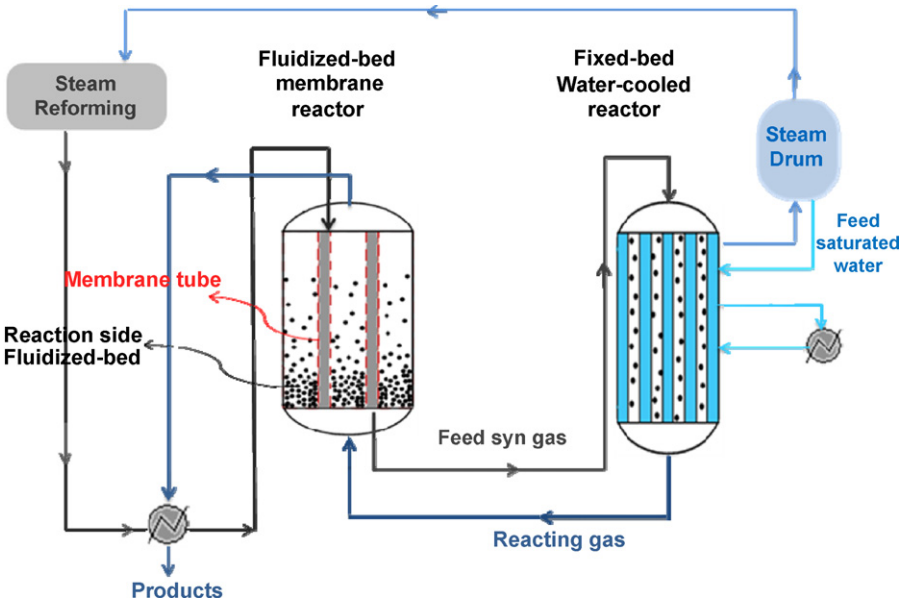

Fig. 2. Schematic diagram of a Fixed-bed cascading with fluidized-bed membrane Fischer–Tropsch reactor (FMD).

considered as dominate FTS reactions [8]:

$$CO + 3H_2 \xrightarrow{R1} CH_4 + H_2O \quad (1)$$

$$2CO + 4H2 \xrightarrow{R2} C2H4 + 2H_2O \quad (2)$$

$$2CO + 5H_2 \xrightarrow{R3} C_2H_6 + 2H_2O \quad (3)$$

$$3CO + 7H_2 \xrightarrow{R4} C_3H_8 + 3H_2O \quad (4)$$

$$4CO + 9H_2 \xrightarrow{R5} n\text{-}C_4H_{10} + 4H_2O \quad (5)$$

$$4CO + 9H_2 \xrightarrow{R6} i\text{-}C_4H_{10} + 4H_2O \quad (6)$$

$$6.05CO + 12.23\,H_2 \xrightarrow{R7} C_{6.05}H_{12.36}(C_5^+) + 6.05\,H_2O \quad (7)$$

$$CO + H_2O \xleftrightarrow{R8} CO_2 + H_2 \quad (\text{WGS reaction}) \quad (8)$$

The reaction rate equation [8] is as follows and the kinetic parameters are given in Table 3:

$$R_t = 0.278 k_t \exp\left(\frac{-Ei}{RT}\right) P_{CO}^m p_{H_2}^n \quad [\text{mol kg}_{\text{cat}}^{-1}\,\text{s}^{-1}] \quad (9)$$

The kinetic model is valid for temperatures between 290 and 310 °C; pressures between 15 and 23 bars and H_2/CO ratio between 0.76 and 1.82 [7].

Table 3
Kinetics parameters data [7].

Reaction no.	m	n	k	E
1	−1.0889	1.5662	142583.8	83423.9
2	0.7622	0.0728	51.556	65018
3	−0.5645	1.3155	24.717	49782
4	0.4051	0.6635	0.4632	34885.5
5	0.4728	1.1389	0.00474	27728.9
6	0.8204	0.5026	0.00832	25730.1
7	0.5850	0.5982	0.02316	23564.3
8	0.5742	0.710	410.667	58826.3

4.2. Fixed-bed cascading with fluidized-bed membrane reactor model (FMD)

4.2.1. Water-cooled reactor (first reactor)

The fixed-bed water-cooled reactor has been modeled according to the following assumptions:

(a) One-dimensional plug flow.
(b) Axial dispersion of heat is negligible compared to convection.
(c) Ideal gas law.

The mass and energy balance equations for gas phase can be written as follows:

$$-\frac{f_{to}}{A_c}\frac{dy_i}{dz} + a_v c_t k_{gi}(y_{is} - y_i) = 0 \quad i = 1, 2, \ldots, N-1 \quad (10)$$

$$-\frac{f_{to}}{A_c} c_{pg}\frac{dT}{dz} + a_v h_f (T_s - T) + \frac{\pi D_i}{A_c} U_{shell}(T_{shell} - T) = 0 \quad (11)$$

where y_i and T are the gas phase mole fraction and temperature, respectively.

The boundary conditions for gas phase equations at inlet of reactor are expressed by

$$z = 0, \qquad y_i = y_{i,in}, \qquad T = T_{in} \quad (12)$$

The mass and energy balance equations for the catalyst pellets can be formulated as follows:

$$k_{gi} a_v c_t (y_i - y_{is}) + \rho_B \eta r_i = 0, \quad i = 1, 2, \ldots, N-1 \quad (13)$$

$$a_v h_f (T - T_s) + \eta \rho_B \sum_{j=1}^{B} r_j (-\Delta H_{fj}) = 0 \quad (14)$$

where y_{is} and T_s are the mole fractions and temperature on the catalyst surface, respectively. Fixed-bed single stage FTS reactor is modeled similar to the above equations for water-cooled reactor of combination reactor system.

4.2.2. Fluidized-bed reactor (second reactor)

4.2.2.1. Tube side (fresh feed synthesis gas). The mass balance equation for hydrogen in tube side is as follows:

$$\frac{f_{to}}{A_c}\frac{dy_h}{dz} + \frac{\alpha_H}{A_s}\left(\sqrt{P_H^t} - \sqrt{P_H^{sh}}\right) = 0 \quad (15)$$

where α_H is the hydrogen permeation rate constant (see Eq. (B-2) in Appendix B), P_H^t and P_H^{sh} are the hydrogen partial pressures in the tube and shell sides, and y_h is the hydrogen mole fraction in the tube side, respectively.

The energy balance equation for tube side is also written as follows:

$$\frac{f_{to}}{A_c}c_{pg_t}\frac{dT_t}{dz}+\frac{\alpha_H}{A_s}\left(\sqrt{P_H^t}-\sqrt{P_H^{sh}}\right)c_{pH}(T-T_t)$$
$$-\frac{\pi D_i}{A_c}U_{tube}(T-T_t)=0 \quad (16)$$

where T_t indicates temperature of synthesis gas in tube side and T is temperature of reacting materials in shell side, respectively.

The boundary conditions at inlet of tubes are as follows:

$$\text{At } z=L,\quad y_i=y_{if},\quad T=T_f \quad (17)$$

4.2.2.2. Shell side (reacting gas flow). Industrial fluidized-bed reactors, especially gas–solid catalytic reactor systems, work often in the bubbling beds [21]. In this study, bubbling regime consisting of two phases namely bubble and emulsion phase is assumed. The two-phase theory of fluidization is used to model and simulate the proposed reactor. This theory suggests that the gas flow rate in the bubble phase is equal to the excess gas flow rate above the amount needed for minimum fluidization. When bubbles rise in a fluidized-bed, the dense (emulsion) phase continues to transfer gas to the rising bubbles. This, in turn, causes the bubbles to grow in size and ascend with higher velocities [22]. The two-phase theory of fluidization assumes that bubble velocity (u_b) remains constant throughout the bed [23]. In a fluidized-bed without internals, a macro-scale circulation pattern prevails with down-flow of the emulsion phase near the wall and up-flow at the center of the bed [24]. In this model, only up-flow of the emulsion phase is considered. This is based on the fact that the reactor exhibits approximately plug flow behavior.

The shell side model has been developed based on the following main assumptions:

(a) Radial distribution of concentration is dispensable.
(b) Due to rapid mixing, the operation is assumed to be isothermal which means bubble and emulsion phases have same temperature.
(c) Both phases are in plug flow regime.
(d) Hydrogen is only added to the emulsion phase.
(e) The axial diffusion of hydrogen through the membrane is neglected compared to the radial diffusion.
(f) Gas flow through the emulsion phase remains constant at minimum fluidization velocity.
(g) In view of small size of the catalyst, the diffusional resistance inside the catalyst particles is neglected.
(h) Catalyst particles can be found in bubble phase and so components can be reacted in rising bubbles, too. But the extension of chemical reactions in bubble phase is much less than emulsion phase.
(i) Ideal gas behavior is assumed.

As can be seen in Fig. 3, an element of length Δz, has been considered. On the basis of the aforementioned assumptions, the bubble and emulsion phase mass conservation equations are formulated as follows:

$$-\delta\frac{f_t}{A_{shell}}\frac{dy_{ib}}{dz}+\delta k_{bei}c_t a_b(y_{ie}-y_{ib})+\delta\gamma\rho_p\sum_{j=1}^{8}r_{bij}=0,$$
$$i=1,2,\ldots,N-1 \quad (18)$$

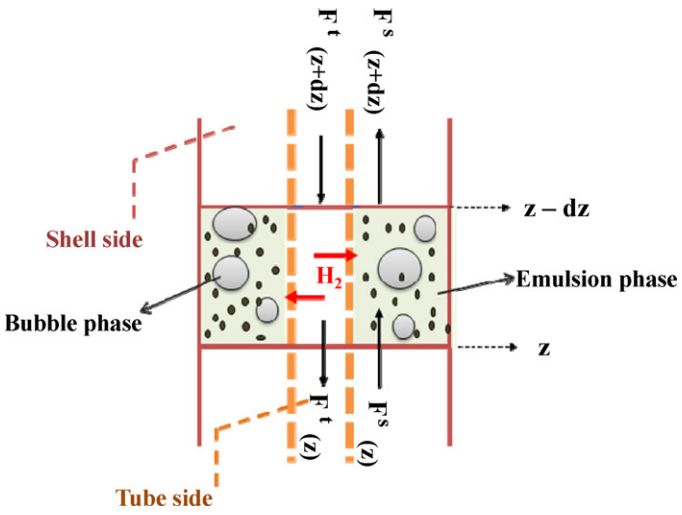

Fig. 3. An element of length, Δz, in fluidized-bed.

$$-(1-\delta)\frac{f_t}{A_{shell}}\frac{dy_{ie}}{dz}+(1-\delta)\rho_e\eta\sum_{j=1}^{8}r_{ij}+\delta k_{bei}a_b c_t(y_{ib}-y_{ie})$$
$$+(1-\delta)\frac{\alpha_H}{A_s}\left(\sqrt{P_H^t}-\sqrt{P_H^{sh}}\right)=0 \quad (19)$$

where y_{ib} and y_{ie} refer to the mole fraction of each component in bubble and emulsion phase, respectively. K_{bei} is mass transfer coefficient between bubble and emulsion phases and γ is volume fraction of catalyst bed occupied by solid particles in the bubble phase. A_{shell} is the equivalent cross-sectional area of shell around each tube.The heat balance equation between the shell and tube of gas-cooled reactor is written by

$$-(1-\delta)\frac{\alpha_H}{A_s}\left(\sqrt{P_H^t}-\sqrt{P_H^{sh}}\right)c_{pH}(T-T_t)+(1-\delta)\eta\rho_e$$
$$\times\sum_{j=1}^{8}r_j(-\Delta H_{fj})+\gamma\rho_B\delta\eta\sum_{j=1}^{8}r_{bj}(-\Delta H_{fj})$$
$$+\frac{\pi D_i}{A_{shell}}U_{shell}(T_t-T)=0 \quad (20)$$

when α_H is zero, the membrane is not permeable to hydrogen and the model is used for fixed-bed cascading with fluidized-bed FTS reactor in which membrane is not applied. The auxiliary and hydrogen permeation correlations are given in Appendixes A and B, respectively and the input data are observed in Tables 1 and 2. The calculated value of effectiveness factor for fixed-bed reactor is equals to 0.9 [25]. The value of effectiveness factor for fluidized-bed reactor is close to unity due to the elimination of diffusional limitations [26].

5. Numerical solution

The governing equations of this model form a set of differential algebraic equations which is consisted of the equations of mass and energy conservative rules. This set of equations has to be coupled with non-linear algebraic equations of the kinetic model, fluidized-bed hydrodynamic properties, transport properties, and other auxiliary correlations. Backward finite difference approximation is applied here to solve this set of equations.

The obtained non-linear algebraic equations are a boundary value problem and have been solved using the shooting method.

The shooting method converts the boundary value problem to an initial value one. The solution is possible by trial and error method. The water and gas-cooled reactors are divided into 19 and 13 nodes, respectively and then Gauss-Newton method is used to solve the non-linear algebraic equations in each node [25]. Matlab programming language is used as application software for numerical simulation [27].

6. Optimization and results

6.1. Model validation

Model validation was carried out by comparison of the proposed model results for fixed-bed single stage FTS reactor with the RIPI pilot plant data [7] under the design specifications and input data. The characteristics of the pilot plant have been tabulated in Tables 1 and 2. Tables 3 and 4 exhibits the model results and the corresponding observed data of the pilot plant. As can be seen, the estimated results are in good agreement with the pilot plant data.

6.2. Optimization

GA is applied to determine the optimal reactor operating conditions for fluidized-bed membrane dual-type concept. Genetic algorithms are mathematical optimization methods that simulate a natural evolution process. The goal of this work is to maximize the C_5^+ production and minimize the CO_2 yield during the operation period. When a single type reactor is converted to two reactors, the ratio of lengths is very important for better results. For exothermic reactions an optimized temperature exists for further production. As illustrated before, in order to reach the highest C_5^+ yield, the H_2/CO usage ratio should be equal or close to the optimum H_2/CO ratio which should be determined. Selection of best possible size of catalyst particles evinces inconsiderable internal diffusion limitations with an insignificant pressure drop and affects minimum fluidization velocity (u_{mf}). Archimedes number and coefficients of mass and heat transfer are presented in Appendix A.

Rising velocity of bubbles (u_b), mass transfer coefficient between bubble and emulsion phase (k_{be}) and specific surface area for bubble (a_b) are a function of bubble diameter. On the other hand, volume fraction of bubble phase to overall volume of bed, δ, and heat transfer coefficient in fluidized-bed side are dependent on bubble velocity (u_b). Minimum fluidization velocity (u_{mf}) and gas phase velocity (u_g) are stated in Appendix A. It seems that an optimum bubble diameter and particle size can almost optimize the whole hydrodynamic parameters. Therefore, substantial improvement in the reactor performance can be achieved by optimizing the temperature profiles, reactors lengths ratio, H_2/CO ratio, catalyst size, shell and tube pressures of second reactor, hydrodynamic parameters and gas phase velocity. For this purpose, 10 parameters are considered as decision variables. The objective function is to maximize the C_5^+ yield and minimize the CO_2 yield, simultaneously. The constraint is the temperature of catalyst beds which should be less than 620 K (catalyst hot spot) along the reactor because at the temperatures higher than 620 K the catalyst will be deactivated. This constraint is stated with penalty function and equals *"weight (hot spot temperature–catalyst temperature)"* in order to obtain the reasonable solution. Thus, optimization problem is formulated as below:

$$\text{Max} f = \frac{C_5^+ \text{ yield}}{CO_2 \text{ yield}} + 10(620 - T_s) \quad (21)$$

$$\text{Path consraint} : T_s < 620\,(\text{K}) \quad (22)$$

Table 4
Comparison between results of fixed-bed model with pilot plant data [7].

Parameter	Pilot plant	Predicted	Error %
X_{CO} (%)	77.94	78.08	0.18
X_{H_2} (%)	92.83	93.48	0.7
C_5^+ selectivity [g/Nm^3(CO + H_2)]	42.55	45.23	6.298
CO_2 selectivity [g/Nm^3(CO + H_2)]	339.07	317.89	−7.22
CH_4 selectivity [g/Nm^3(CO + H_2)]	44.15	46.23	4.71
H_2O selectivity [g/Nm^3(CO + H_2)]	120.67	117.8	−3.38
C_2H_4 selectivity [g/Nm^3(CO + H_2)]	3.95	4.22	6.83
C_2H_6 selectivity [g/Nm^3(CO + H_2)]	11.78	10.7	−9.168
n-C_4 selectivity [g/Nm^3(CO + H_2)]	11.07	9.65	−12.82
i-C_4 selectivity [g/Nm^3(CO + H_2)]	14.45	12.19	−15.46
C_3H_8 selectivity [g/Nm^3(CO + H_2)]	9.33	7.82	−16.18

Table 5
The optimized parameters for the proposed FTS reactor system.

T_{shell} (K)	540
T_f (K)	567
L_{ratio}	1.88
H_2/CO ratio	1.02
P_t (bar)	57
P_s (bar)	22
d_p (mm)	0.154
$d_{b,ave}$ (cm)	3.2
u_b (m/s)	0.813
u_{mf} (m/s)	0.078
u_g (m/s)	0.492
A_{shell} (m^2)	0.005
$V_{reactor}$ (m^3)	0.0262
N	25

6.3. Optimization results

The optimization was carried out and the results are summarized in Table 5. The simulation of fixed-bed cascading with fluidized-bed membrane configuration is carried out by use of the optimization results in Table 5. Simulation of the suggested FTS reactor concept using the optimization results shows 19.6% additional C_5^+ yield in OFMD relative to FMD system.

Fig. 4 shows the objective function at optimized and non-optimized conditions as a function of reactor length.

Fig. 5 shows the effects of optimization results on the fluidization behavior. Fig. 5(a) displays bubble diameter profile along the height of fluidized-bed according to Werther correlation. Using optimized parameters, the bubble size becomes less than non-optimized system. Since the bubble rising velocity is correlated with bubble

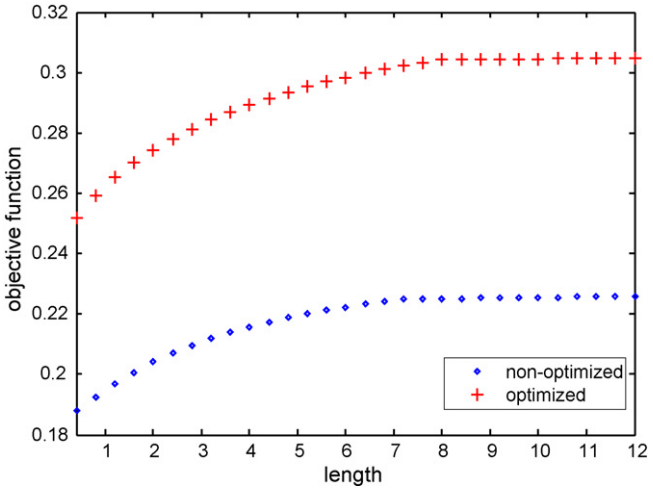

Fig. 4. Objective function vs. length of reactor.

diameter as stated by Eq. (A-9), rising velocity for optimized system is lower than non-optimized system as shown in Fig. 5(b). Fig. 5(c) shows the mass transfer coefficient between bubble and emulsion phase along the reactor for C_5^+ is higher than values for non-optimized system. Mass transfer coefficient is inversely proportional to bubble diameter as stated by Eq. (A-12) so that optimized mass transfer coefficients of each components such as C_5^+ is higher than non-optimized mass transfer coefficients.

Fig. 5(d) shows fraction of bed occupied by bubble phase in optimized and non-optimized systems. This parameter is a function of rising bubble, gas phase velocity and minimum fluidization velocity. Finally Fig. 5(e) clarifies that there is an improvement of heat transfer coefficient along the reactor for optimized conditions.

Fig. 6 shows a comparison between different types of FTS reactors discussed in this research. This figure presents the profiles of yields of FTS products along the FixS, OFD and OFMD. According

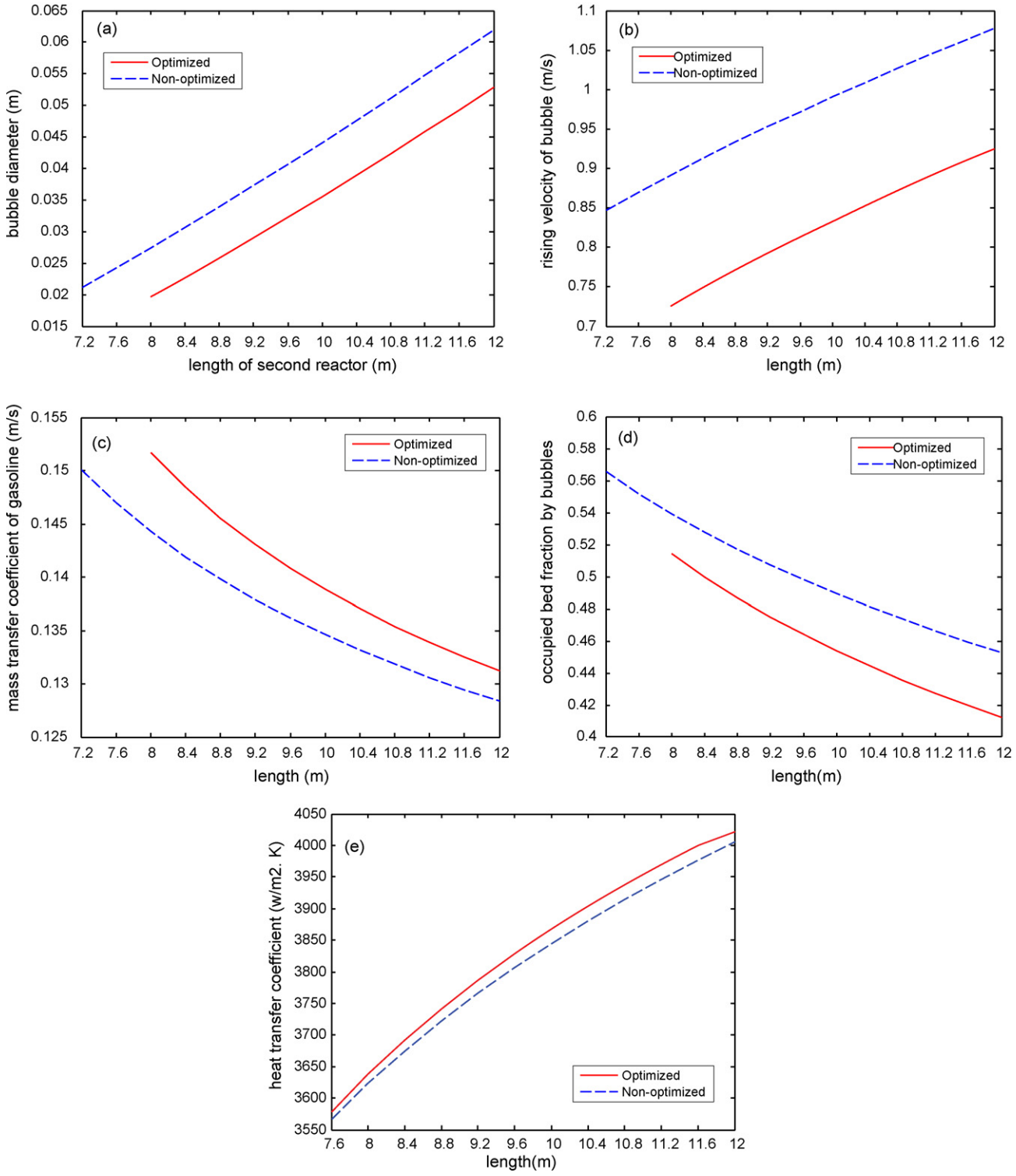

Fig. 5. Comparison of (a) bubble diameter, (b) rising bubble velocity, (c) mass transfer coefficient of gasoline, (d) fraction of bed occupied with bubble phase, and (e) heat transfer coefficient profiles along the reactor for optimized and non-optimized systems.

to Fig. 6(a), the C_5^+ yield obtained by the optimized fluidized-bed membrane dual-type system is remarkably higher than fixed-bed single stage FTS reactor. Also, this figure confirms the 45.9% additional yield of C_5^+ in OFMD respect to FixS. Obviously, the small difference between OFMD and OFD performances is attributed to the positive effect of applying membrane in OFMD. Carbon dioxide is produced by the equilibrium water–gas-shift (WGS) reaction and CO_2 is converted to FTS products as well. At the higher tem-

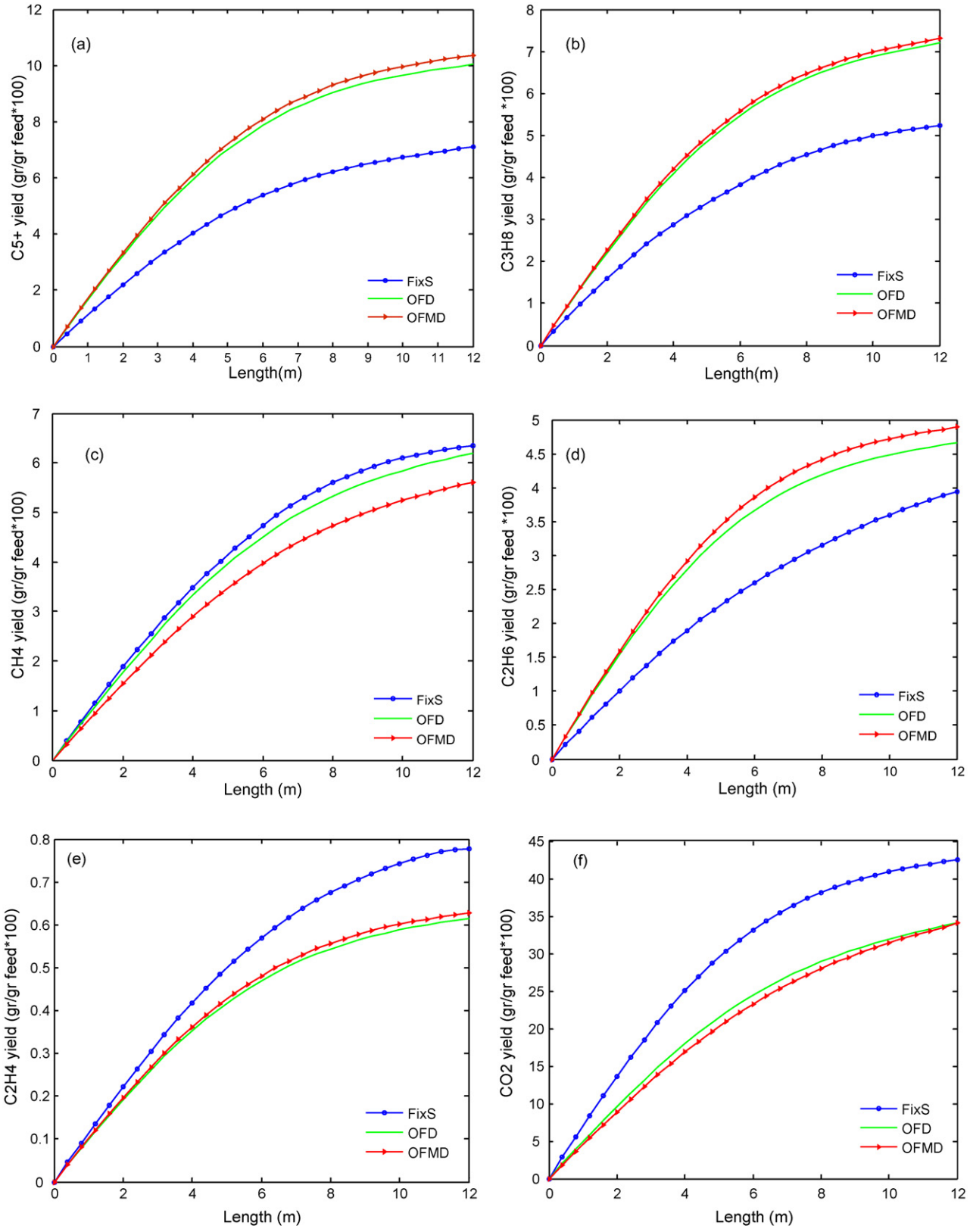

Fig. 6. Comparison of production yield profiles for (a) C_5^+, (b) C_3H_8, (c) CH_4, (d) C_2H_6, (e) C_2H_4, (f) CO_2, (g) iso-butane and (h) normal butane along the three different types of reactors.

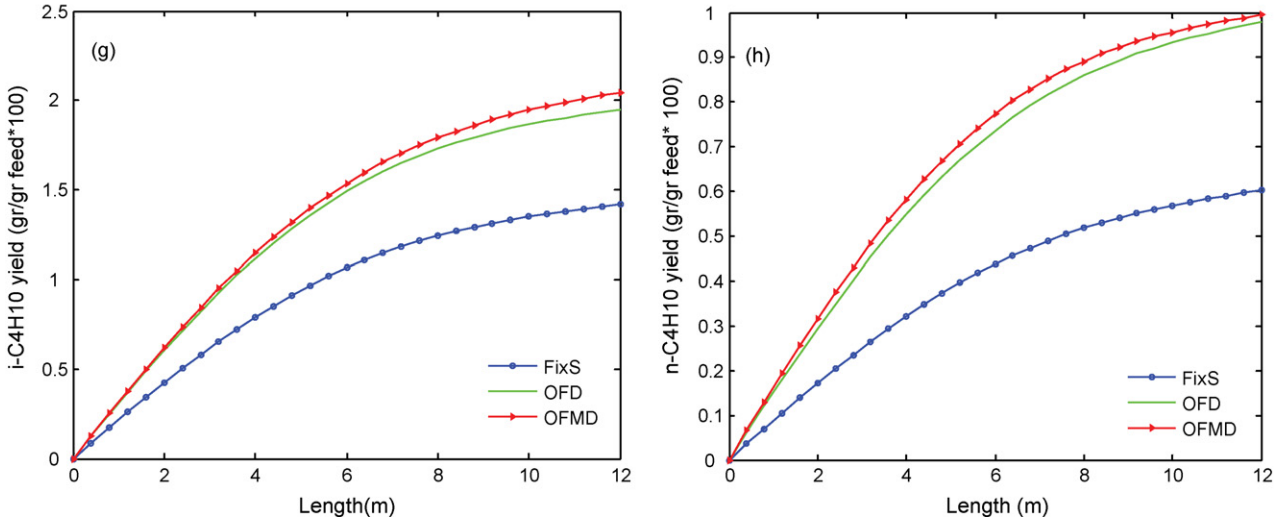

Fig. 6. (*Continued*).

peratures used in the HTFT process, the WGS reaction is rapid and goes to equilibrium, which allows CO_2 to be converted to FTS products as well. Fig. 6(f) clearly shows that the performance of OFMD system suppresses the formation of the undesired products, CO_2, and thus enhances production of the desired hydrocarbon products. As seen in Fig. 6(a), (b), (d), (g) and (h), the highest propane, ethane, normal butane, isobutene and C_5^+ production is related to OFMD reactor system but the most production of ethylene is resulted by FixS system. Methane is often not regarded as a product, especially not if natural gas is the feedstock. Therefore, methane is often reformed back to synthesis gas and then fed to the FTS reactor again [29]. Fig. 6(c) represents methane yield production along the three types of reactors. The most and least methane production is observed in FixS and OFMD systems, respectively. Consequently, from FTS products distribution standpoint, fixed-bed cascading with fluidized-bed membrane reactor in optimized conditions can be the most favorable configuration.

Fig. 7 illustrates the comparison of hydrogen and carbon monoxide conversion for OFMD, OFD and FixS. As shown in this figure, OFMD has several advantages over OFMD, OFD and FixS systems. These advantages are lower pressure drop, lower mass transfer limitations due to very small particle size, and control dozing of the hydrogen partial pressure along the reactor so that the utmost conversion of reactants is achieved by OFMD.

As understood from Fig. 7(a), hydrogen consumption in the first half of the reactors is relatively high. Therefore, there might be a leak of hydrogen in the second section of reactors. Adding hydrogen to H_2-poor reacting gas through the Pd–Ag membrane also leads to more conversion of reactants and so more production of hydrocarbons.

Fluidized-bed system eliminates the radial and axial temperature gradients due to excellent heat transfer characteristics. Fixed-beds have relatively poor heat transfer coefficient as compared to fluidized-beds, thus the control of their temperature profiles are more difficult. The temperature uniformity as a result of very good heat transfer and temperature equalization characteristics of fluidized-bed improves the products distribution. Heavy products on the catalyst pellets in fluidized-bed and HTFT system can be deposited and leads to more C_5^+ and linear low molecular-mass olefins production.

Fig. 8 compares the reacting gas temperature of different reactor types. As it is shown in this figure control of temperature in OFMD reactor system is easier and the risk of hotspot and temperature runaway is least. The processing gas temperature of FMD configu-

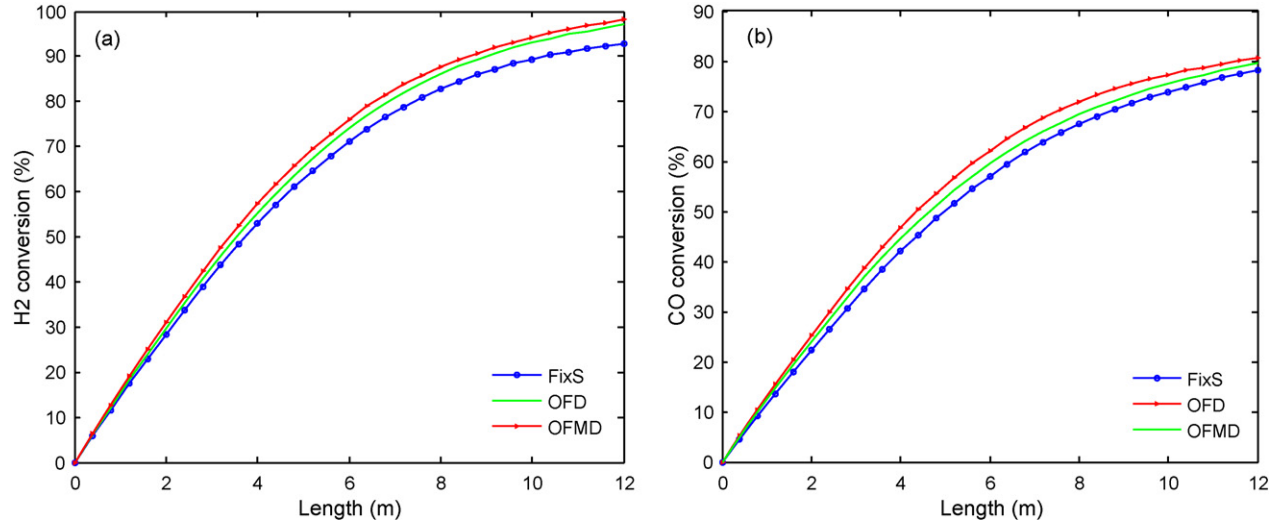

Fig. 7. Comparison of (a) H_2 conversion and (b) CO conversion profiles along the three different FT systems.

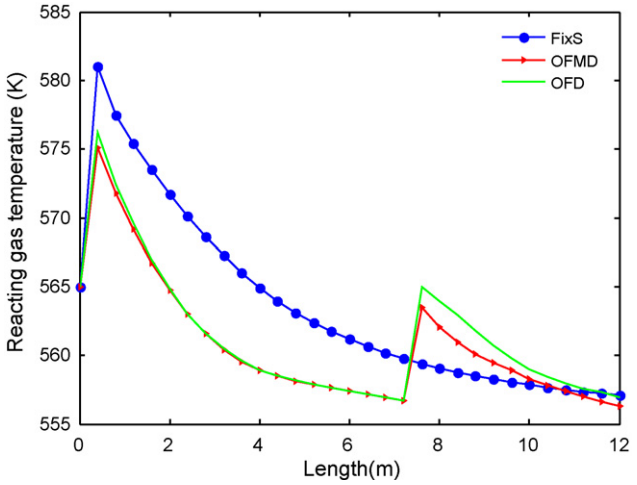

Fig. 8. Comparison of reacting gas temperature profiles along the three different types of FT systems.

ration was optimized using the results of feed and cooling water temperature optimization.

Fig. 9 displays the coolant temperature along the three types of mentioned FTS systems. In combination of fixed and fluidized-bed reactor configurations there are two different coolants. The first coolant is fresh synthesis gas in gas-cooled reactor and the second coolant is saturated water in water-cooled reactor which is converted to saturated steam due to thermal exchange with reaction side. Thus, a horizontal line is resulted for coolant temperature profile along the water-cooled reactor as shown in Fig. 9. Also the fresh synthesis gas is heated as moves along the tubes of gas-cooled reactor and is prepared to reach to suitable temperature for initiation of reaction in water-cooled reactor. Due to heating of fresh synthesis gas by heat of reaction the need for a large pre-heater is eliminated.

Fig. 10 displays the hydrogen permeation rate profile along the fixed-bed cascading with fluidized-bed membrane reactor in optimized and non-optimized conditions. As presented in Appendix B, hydrogen permeation flux depends on H_2 partial pressure difference between two sides, membrane thickness, tube length and synthesis gas temperature. According to Arrhenius law, increasing temperature promotes hydrogen permeability. Fig. 10 introduces optimized system as the pre-eminent system with a view to hydrogen permeation rate. Applying optimum values of shell and tube

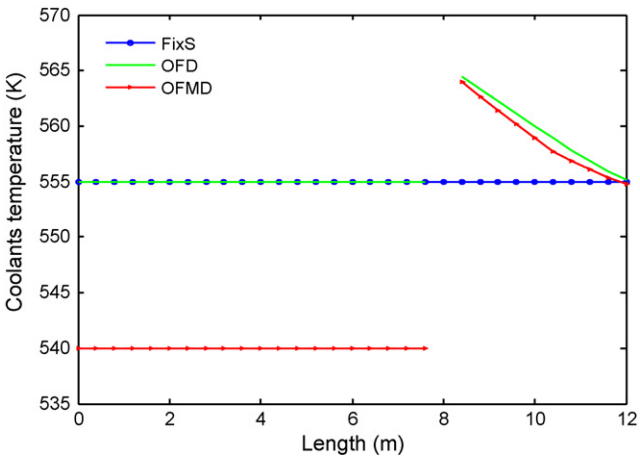

Fig. 9. Comparison of coolant temperature profiles along the three different types FT systems.

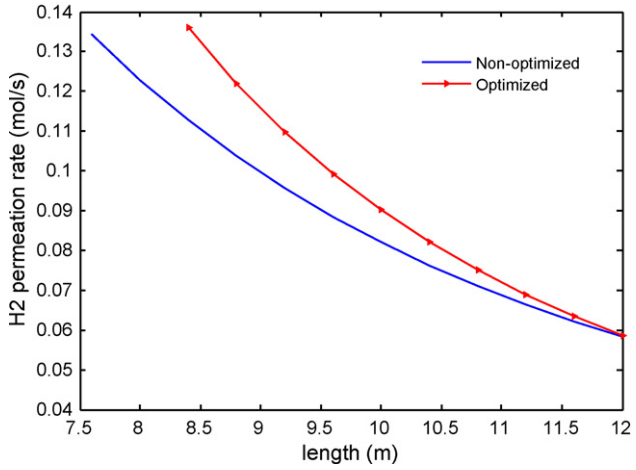

Fig. 10. Hydrogen permeation rate profile for optimized and non-optimized system.

pressures, reactor length and temperatures (listed in Table 5) increases the hydrogen permeation rate remarkably.

A comparison of carbon molar selectivity of products between FixS, OFD and OFMD configurations is presented in Fig. 11. Here, carbon molar selectivity of each component is defined as [22]:

$$S = \frac{\text{moles of C\_atom in product}}{\text{moles of CO consumed}} \times 100\% \quad (23)$$

According to this comparison, the combination of fixed-bed and membrane assisted fluidized-bed concept in optimized conditions enhances the C_5^+ selectivity and likely declines methane and carbon dioxide selectivity. Therefore OFMD exhibits the best results, whether for desired products or undesired products.

Fig. 12 shows a comparison of yield profiles [g(reactor volume)$^{-1}$ h^{-1}] of C_5^+, i-C_4H_{10}, CO_2 and CH_4 along the FixS and OFMD. The equivalent volume of the fixed-bed cascading with fluidized-bed membrane configuration in optimized conditions (for each tube) is about 1.5-fold of the volume of fixed-bed single stage FTS reactor.

Above figures demonstrate an enhancement in C_5^+ production about 1.7% and a significant decrease in CO_2 and CH_4 production, in terms of [g m^{-3} h^{-1}]. Some considerable features of the fixed-bed cascading with fluidized-bed membrane reactor like higher production of C_5^+ and properly products distribution suggest that the proposed concept in optimized conditions is an interesting candi-

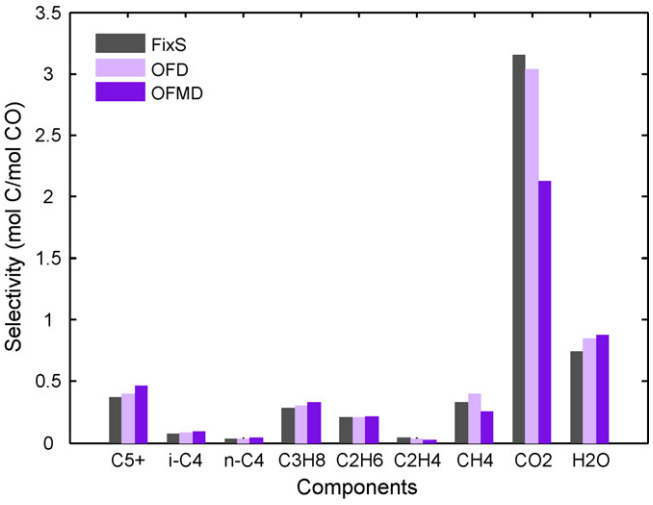

Fig. 11. A comparison between products selectivities of various reactor systems.

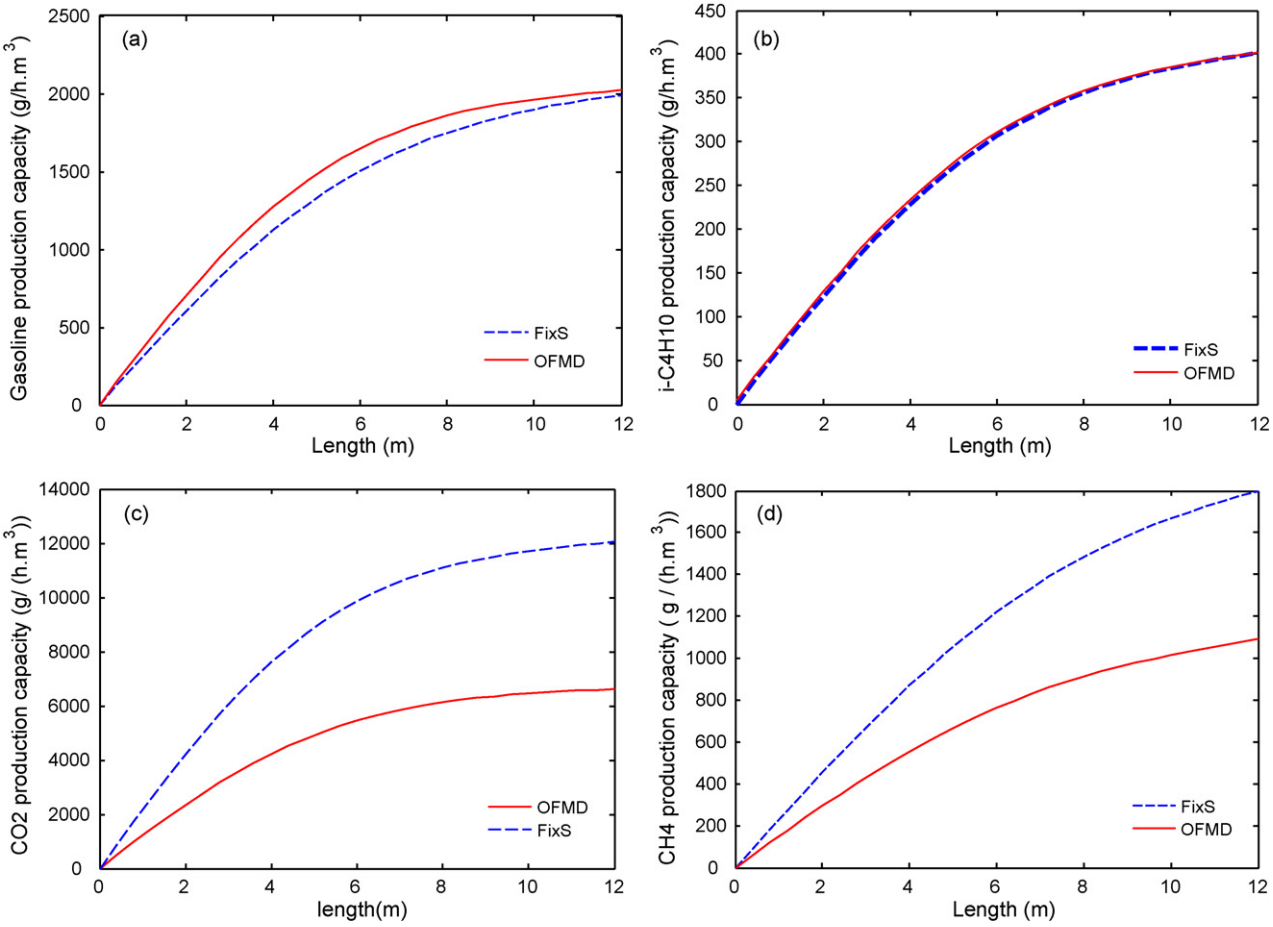

Fig. 12. Production capacities profiles of (a) C_5^+, (b) *i*-C_4H_{10}, (c) CO_2 and (d) CH_4 along the FixS and OFMD [g m^{-3} h^{-1}].

date for application in Fischer–Tropsch synthesis. However, from an industrial point of view there are still many issues to be addressed before putting a case for successful commercialization. These issues are difficulties in reactor construction, erosion of reactor internals, catalyst attrition due to high flow velocities in fluidization regime, the cost of CO_2 capture, the cost of membranes and their fouling and sealing in the fluidization conditions.

7. Conclusion

A novel fixed-bed cascading with fluidized-bed membrane configuration for Fischer–Tropsch synthesis was optimized to increase C_5^+ production yield and decrease byproducts. The potential possibilities of the different configurations of cascading FTS reactors were analyzed using one-dimensional packed bed model for first reactor and two phase bubbling model in second reactor to obtain the necessary comparative estimates. The mathematical model was validated against the RIPI pilot plant data and then optimized to maximize C_5^+ production and minimize CO_2 yield. The optimization method used is based on Genetic Algorithms. C_5^+ to CO_2 yield ratio was considered as optimization criterion to be maximized; also, 10 variables are tuned. Lastly, optimization results were compared with results of fixed-bed single stage FTS reactor. This comparison shows 1.7% in terms of [g(reactor volume)$^{-1}$ h^{-1}] or 45.9% in terms of [g/g feed × 100] additional C_5^+ yield and also a significant decrease in formation of CO_2 along the OFMD reactor. These features suggest that the proposed concept can be an interesting candidate for producing C_5^+ from synthesis gas. Nevertheless, an investigation in relation to the environmental impacts, commercial viability and economic of the proposed configuration is necessary to be commercialized.

Acknowledgements

The authors thank Research Institute of Petroleum Industry of Iran (RIPI) for providing the valuable pilot plant data. The authors gratefully appreciate financial support by Iranian Central Oil Field Company during completion of this work. Also the corresponding author would like to appreciate financial support by Shiraz University and University of Newcastle, Australia during initiation of this work in his sabbatical leave.

Appendix A. Auxiliary correlations

A.1. Fixed-bed reactor correlations

The mass transfer coefficients between the gas phase and the solid phase in fixed-bed reactor (first reactor) have been taken from Cussler [24]:

$$k_{gt} = 1.17 Re^{-0.42} Sc_t^{-0.67} u_g \times 10^3 \quad \text{(A-1)}$$

$$Re = \frac{2R_p u_g}{\mu} \quad \text{(A-2)}$$

$$Sc_i = \frac{\mu}{\rho D_m^i 10^{-4}} \tag{A-3}$$

The diffusivity of each component in the gas mixture is given by [30]:

$$D_{im} = \frac{1 - y_i}{\sum_{i \neq j}(y_i/D_{ij})} \tag{A-4}$$

$$D_{ij} = \frac{10^{-7} T^{3/2} \sqrt{(1/M_i) + (1/M_j)}}{P\left(v_{ci}^{3/2} + v_{cj}^{3/2}\right)^2} \tag{A-5}$$

where D_{ij} is the binary diffusivity calculated using the Fuller–Schetter–Giddins equation [25]. M_i and v_{ci} are the molecular weight and critical volume of component i.

The overall heat transfer coefficient between the circulating boiling water of the shell side and the bulk of the gas phase in the tube side is given by the following correlation:

$$\frac{1}{U_{shell}} = \frac{1}{h_i} + \frac{A_i \ln(D_o/D_i)}{2\pi L K_w} + \frac{A_i}{A_o}\frac{1}{h_o} \tag{A-6}$$

where h_i is the convection heat transfer coefficient between the gas phase and the reactor wall and is obtained by the following correlation [26]:

$$\frac{h_i}{c_p \rho \mu}\left(\frac{c_p \mu}{\kappa}\right)^{2/3} = \frac{0.458}{\varepsilon_B}\left(\frac{\rho u d_p}{\mu}\right)^{-0.407} \tag{A-7}$$

where ε_B is the void fraction of the catalytic bed and d_p is the equivalent catalyst diameter and the other parameters are related to bulk gas phase.

To calculate the heat transfer coefficient of boiling water in the shell side at high pressure, Leva correlation is applied [25]:

$$h_o = 282.2 P^{4/3} \Delta T^2, \qquad 0.7 < P < 14\,\text{MPa} \tag{A-8}$$

A.2. Fluidized-bed reactor correlations

The empirical correlations for the hydrodynamic parameters used in the proposed model have been taken from the literature, although they were originally obtained for beds without internals.

Based on two-phase theory, Harrison and Davidson suggested the following correlation for the rising velocity of bubbles [28]:

$$u_b = u_0 - u_{mf} + 0.711(g d_b)^{0.5} \tag{A-9}$$

The following correlation has been selected for minimum fluidization velocity [23]:

$$u_{mf} = \left(\frac{\mu_g}{\rho_g d_p}\right)\left(\sqrt{27.2^2 + 0.0408 Ar} - 27.2\right) \tag{A-10}$$

where Ar is Archimedes number.

The following correlation is used to calculate the bubble diameter at each height of a catalytic bed [28]:

$$d_b = 0.00853(1 + 0.272(u_0 - u_{mf}))^{1/3}(1 + 0.0684z)^{1.21} \tag{A-11}$$

The mass transfer coefficient between the bubble phase and the emulsion phase in fluidized-bed reactor is expressed by [24]:

$$k_{bei} = 0.75 u_{mf} + \left(\frac{g {D_{mi}}^2}{d_b}\right)^{0.25} \tag{A-12}$$

where D_m is the diffusivity of each component in the gas mixture. The heat transfer coefficient between the bubble phase and the emulsion phase in fluidized-bed reactor is written as follows:

$$h = h_g + h_r + (1 - \delta)\left(\frac{2k_{ew}^0}{d_p} + 0.05 c_{pg} \rho_g u_0\right) \tag{A-13}$$

where h_g and h_r are convection and radiation heat transfer coefficient, respectively. k_{ew}^0 is the effective conductivity of a thin layer of bed near the wall surface and δ is the fraction of bed occupied by bubble phase as follows [28]:

$$\delta = \frac{u - u_{mf}}{u_b + u_{mf}} \tag{A-14}$$

Appendix B. Hydrogen permeation correlations

The flux of hydrogen permeating through the palladium membrane, j_H, will depend on the hydrogen partial pressure difference between the two sides of the membrane. Here, the hydrogen permeation is determined assuming the Sieverts law [29]:

$$j_H = \alpha_H\left(\sqrt{P_H^t} - \sqrt{P_H^{sh}}\right) \tag{B-1}$$

where α_H is hydrogen permeation rate constant and is defined as [31]:

$$\alpha_H = \frac{2\pi L \bar{p}}{\ln(R_o/R_i)} \tag{B-2}$$

where R_o and R_i stand for outer and inner radius of Pd–Ag layer. Here, the hydrogen permeability through Pd–Ag layer is determined assuming the Arrhenius law, which is a function of temperature as follows [32]:

$$\bar{p} = p_0 \exp\left(\frac{-E_p}{RT}\right) \tag{B-3}$$

where the pre-exponential factor p_0 above 200 °C is reported as 6.33×10^{-8} mol m^{-2} s^{-1} Pa$^{-1/2}$ and activation energy E_p is 91270 kJ/kmol [32].

Appendix C. Nomenclature

Symbol	Unit	Definition
A_c	m^2	Cross-sectional area of each tube
A_i	m^2	Inner area of each tube
A_s	m^2	Lateral area of each tube
A_{shell}	m^2	Cross-sectional area of shell
a_b	m^2	Interface area between bubbles and emulsion phase
a_v	m^2 m^{-3}	Specific surface area of catalyst pellet
c_{Pg}	J mol^{-1} K^{-1}	Specific heat of the gas at constant pressure
c_{Pg_t}	J mol^{-1} K^{-1}	Specific heat of the gas inside the tube at constant pressure
c_{pH}	J mol^{-1} K^{-1}	Specific heat of hydrogen at constant pressure
c_{Ps}	J mol^{-1} K^{-1}	Specific heat of the catalyst at constant pressure
c_t	mol m^{-3}	Total concentration
D_i	m	Tube inside diameter
D_{ij}	m^2 s^{-1}	Binary diffusion coefficient of component i in component j
D_m^i	m^2 s^{-1}	Diffusion coefficient of component i in the mixture
D_o	m	Tube outside diameter
d_p	m	Particle diameter
h_f	W m^{-2} K^{-1}	Gas-catalyst heat transfer coefficient
h_i	W m^{-2} K^{-1}	Heat transfer coefficient between fluid phase and reactor wall
h_o	W m^{-2} K^{-1}	Heat transfer coefficient between coolant stream and reactor wall
F_t	mol s^{-1}	Total molar flow rate in shell side
f_{t0}	mol s^{-1}	Total molar flow rate in tube side
K	W m^{-1} K^{-1}	Conductivity of fluid phase
K_w	W m^{-1} K^{-1}	Thermal conductivity of reactor wall
k_{gi}	m s^{-1}	Mass transfer coefficient between gas and solid phase for component i
k_{bei}	m s^{-1}	Mass transfer coefficient between bubble and emulsion phase for component i
L	m	Length of reactor

Appendix C (*Continued*)

Symbol	Unit	Definition
M_i	g mol^{-1}	Molecular weight of component *i*
N	–	Number of components
P_H^t	bar	Tube side pressure
P_H^{sh}	bar	Shell side pressure
$\bar{p}$	mol m^{-1} s^{-1} Pa$^{-1/2}$	Permeability of hydrogen through Pd–Ag layer
p_0	mol m^{-1} s^{-1} Pa^{-1}	Pre-exponential factor of hydrogen permeability
R	J mol^{-1} K^{-1}	Universal gas constant
Re	–	Reynolds number
R_i	m	Inner radius of Pd–Ag layer
R_o	m	Outer radius of Pd–Ag layer
r_i	mol kg^{-1} s^{-1}	Reaction rate of component *i*
r_{bi}	mol kg^{-1} s^{-1}	Reaction rate of component *i* in bubble phase
Sc_i	–	Schmidt number of component *i*
T	K	Bulk gas phase temperature
T_s	K	Temperature of solid phase
T_{shell}	K	Temperature of coolant stream in first reactor
T_t	K	Temperature of coolant stream in second reactor
U_{shell}, U_{tube}	W m^{-2} K^{-1}	Overall heat transfer coefficient between coolant and process streams
u_g	m s^{-1}	Linear velocity of gas phase
u_b	m s^{-1}	Rising bubble velocity
y_i	mol mol^{-1}	Mole fraction of component *i* in the fluid phase
y_{is}	mol mol^{-1}	Mole fraction of component *i* in the solid phase
y_{ie}	mol mol^{-1}	Mole fraction of component *i* in the emulsion phase
y_{ib}	mol mol^{-1}	Mole fraction of component *i* in the bubble phase
z	m	Axial reactor coordinate
Greek letters		
α_H	mol m^{-1} s^{-1} Pa$^{-0.5}$	Hydrogen permeation rate constant
$\Delta H_{f,i}$	J mol^{-1}	Enthalpy of formation of component *i*
ΔH_{298}	J mol^{-1}	Enthalpy of reaction at 298 K
δ	–	Bubble phase fraction
ε_B	–	Void fraction of catalytic bed
ε_s	–	Void fraction of catalyst
ε_{mf}	–	Void fraction of bed at minimum fluidization
γ	–	Volume fraction of catalyst occupied by solid particles in bubble
μ	kg m^{-1} s^{-1}	Viscosity of fluid phase
v_{ci}	cm^3 mol^{-1}	Critical volume of component *i*
ρ	kg m^{-3}	Density of fluid phase
ρ_B	kg m^{-3}	Density of catalytic bed
ρ_e	kg m^{-3}	Density of emulsion phase
ρ_p	kg m^{-3}	Density of catalyst
η	–	Catalyst effectiveness factor

Superscripts and subscripts	
f	Feed conditions
in	Inlet conditions
out	Outlet conditions
s	Catalyst surface
sh	Shell side
e	Emulsion phase
b	Bubble phase
t	Tube side

References

[1] K.Y. Koo, H.S. Roh, Y.T. Seo, D.J. Seo, W.L. Yoon, S. Bin Park, A highly effective and stable nano-sized Ni/MgO–Al_2O_3 catalyst for gas to liquids (GTL) process, International Journal of Hydrogen Energy 33 (8) (2008) 2036–2043.

[2] A. Fabiano, N. Fernandes, Optimization of Fischer–Tropsch synthesis using neural networks, Chemical Engineering and Technology 29 (4) (2006) 449–453.

[3] M.V. Cagnoli, N.G. Gallegos, A.M. Alvarez, J.F. Bengoa, A.A. Yeramián, M. Schmal, S.G. Marchetti, Catalytic CO hydrogenation on potassic Fe/zeolite LTL, Applied Catalysis A: General 230 (2002) 169.

[4] Y.-N. Wang, Y.-Y. Xu, Y.-W. Li, Y.-L. Zhao, B.-J. Zhang, Heterogeneous modeling for fixed-bed Fischer–Tropsch synthesis: reactor model and its applications, Chemical Engineering Science 58 (2003) 867–875.

[5] A. Akhtar, V.K. Pareek, M.O. Tade, Modern trends in CFD simulations: application to GTL technology, Chemical Product and Process Modeling 1 (1) (2006), Art. No. 2.

[6] C.S. Patil, M. Van Sint Annaland, J.A.M. Kuipers, Design of a novel autothermal membrane-assisted fluidized-bed reactor for the production of ultra pure hydrogen from methane, Industrial and Engineering Chemistry Research 44 (25) (2005) 9502–9512.

[7] Fischer–Tropsch pilot plant of Research Institute of Petroleum Industry and National Iranian Oil Company (RIPI-NIOC), Tehran 18745-4163, Iran, 2004.

[8] M.A. Marvast, M. Sohrabi, S. Zarrinpashneh, G. Baghmisheh, Fischer–Tropsch synthesis: modeling and performance study for Fe-HZSM5 bifunctional catalyst, Chemical Engineering and Technology 28 (1) (2005) 78–86.

[9] M.R. Rahimpour, H. Elekaei, A comparative study of combination of Fischer–Tropsch synthesis reactors with hydrogen-permselective membrane in GTL technology, Fuel Processing Technology 90 (6) (2009) 747–761.

[10] A.A. Forghani, H. Elekaei, M.R. Rahimpour, Enhancement of gasoline production in a novel hydrogen-permselective membrane reactor in Fischer–Tropsch synthesis of GTL technology, International Journal of Hydrogen Energy 34 (9) (2009) 3965–3976.

[11] M.R. Rahimpour, M. Lotfinejad, Enhancement of methanol production in a membrane dual-type reactor, Chemical Engineering and Technology 30 (8) (2007) 1062–1076.

[12] A.P. Steynberg, M.E. Dry, B.H. Davis, B.B. Breman, Fischer–Tropsch reactors, Studies in Surface Science and Catalysis 152 (2004) 64–195.

[13] F. Gallucci, A. Basile, A theoretical analysis of methanol synthesis from CO_2 and H_2 in a ceramic membrane reactor, International Journal of Hydrogen Energy 32 (2007) 5050–5058.

[14] M.E.E. Abashar, Coupling of steam and dry reforming of methane in catalytic fluidized bed membrane reactors, International Journal of Hydrogen Energy 29 (2004) 799–808.

[15] A.M. Adris, J.R. Grace, Characteristics of fluidized-bed membrane reactors: scale-up and practical issues, Industrial and Engineering Chemistry Research 36 (1997) 4549–4556.

[16] Y.A. Liu, M. Arthur, Squires, Kenneth Konrad, FTS from a low H_2/CO gas in a dry fluidized bed system, DE83011185, 1983.

[17] M.E. Dry, Practical and theoretical aspects of the catalytic Fischer–Tropsch process, Applied Catalysis A: General 138 (2) (2004) 319–344.

[18] F. Askari, M.R. Rahimpour, A. Jahanmiri, A. Khosravanipour Mostafazadeh, Dynamic simulation and optimization of dual-type methanol reactor using genetic algorithms, Chemical Engineering and Technology 31 (4) (2008).

[19] M.R. Rahimpour, H. Elekaei Behjati, Dynamic optimization of membrane dual-type methanol reactor in the presence of catalyst deactivation using genetic algorithm, Fuel Processing Technology 90 (2) (2009) 279–291.

[20] M.R. Rahimpour, M. Lotfinejad, A comparison of co-current and counter-current modes of operation for a membrane dual-type methanol reactor, Chemical Engineering and Processing: Process Intensification 47 (9–10) (2007) 1819–1830.

[21] O. Levenspiel, Chemical Reaction Engineering, John Wiley & Sons, New York, 1999.

[22] J. Chang, L. Bai, B. Teng, R. Zhang, J. Yang, Y. Xu, H. Xiang, Y. Li, Kinetic modeling of Fischer–Tropsch synthesis over Fe–Cu–K–SiO_2 catalyst in slurry phase reactor, Chemical Engineering Science 62 (2007) 4983–4991 (18-20 SPEC. ISS.).

[23] S.A.R.K. Deshmukh, J.A. Laverman, A.H.G. Cents, M. van Sint Annaland, J.A.M. Kuipers, Development of a membrane-assisted fluidized bed reactor. 1. Gas phase back-mixing and bubble-to-emulsion phase mass transfer using tracer injection and ultrasound experiments, Industrial and Engineering Chemistry Research 44 (2005) 5955–5965.

[24] E.L. Cussler, Diffusion, Mass Transfer in Fluid Systems, Cambridge University Press, Cambridge, 1984.

[25] M. Panahi, Master's thesis, Sharif University of Technology, 2005.

[26] K.M. Wagialla, S.S.E.H. Elnashaie, Fluidized-bed reactor for methanol synthesis. A theoretical investigation, Industrial and Engineering Chemistry Research 30 (10) (1991) 2298–2308.

[27] L.F. Shampine, M.W. Reichelt, The MATLAB ODE Suite, SIAM Journal on Scientific Computing 18 (1977) 1–12.

[28] D. Kunii, O. Levenspiel, Fluidization Engineering, Wiley, New York, 1991.

[29] S. Lögdberg, Master's thesis, KTH Sweden School of Chemical Science and Engineering, 2007.

[30] C.R. Wilke, Chemical Engineering and Processing 45 (1949) 218.

[31] M.R. Rahimpour, A. Khosravanipour Mostafazadeh, M.M. Barmaki, Application of hydrogen-permselective Pd-based membrane in an industrial single-type methanol reactor in the presence of catalyst deactivation, Fuel Processing Technology 89 (12) (2008) 1396–1408.

[32] M.R. Rahimpour, S. Ghader, Enhancement of CO conversion in a novel Pd–Ag membrane reactor for methanol synthesis, Chemical Engineering and Processing 43 (2004) 1181–1188.